Fracture energy of high performance concrete at temperatures up to 450°C

B.Zhang & N.Bicanic
Department of Civil Engineering, University of Glasgow, Glasgow G12 8LT, The United Kingdom

ABSTRACT: Fracture energy of high performance concrete was studied by conducting three-point bending tests on 101 beams of 500 × 100 × 100 mm at high temperatures up to 450°C (*hot*) and in cooled-down states (*cold*). Fracture energy sustained a decrease-increase tendency with increasing heating temperature for the *hot* concrete but an increase-decrease tendency for the *cold* concrete. Modulus of rupture decreased with heating temperature for the *hot* concrete but sustained an increase-decrease tendency for the *cold* concrete. Residual compressive and tensile strengths and Young's modulus decreased with heating temperature. A sudden drop was experienced for all strength parameters at around 150°C. Fast cooling further decreased all properties except Young's Modulus. Weight loss monotonically increased with heating temperature at the beginning but a hygric equilibrium state could be reached eventually. Fast cooling led to a slightly higher ultimate weight loss. Fracture energy and other material properties could be closely related to the ultimate weight loss.

1 INTRODUCTION

In designing special concrete structures subject to high temperature environment, e.g. prestressed concrete pressure vessels in nuclear industry, the information about fundamental properties such as strength, stiffness and toughness under highly elevated temperatures is very often required. More extensive research into these fracture properties at high temperatures only started in the late 1970's and has since become progressively an area of research interest (Schneider, 1988, Bazant & Kaplan, 1996).

Exposure to elevated temperatures physically causes large volume changes due to thermal dilations, thermal shrinkage and creep associated with the loss of water, leading to large internal stresses and micro cracking and fractures. Rapid exposure to high temperatures with high pressures also leads to explosive spalling of concrete. High temperatures cause chemical and micro-structural changes, such as migration of water (diffusion, drying), increased dehydration, interfacial thermal incompatibility and chemical decomposition of hardened cement paste and aggregates. All these changes decrease both strength and stiffness and increase irreversible deformation and damage. Many references tentatively acknowledge that the changes in fracture properties at high temperatures are related to the evaporation of moisture in concrete, physically and/or chemically. However, the effect of moisture in concrete on these fracture properties at high temperatures has not been systematically investigated. Water does not simply

make up a volume proportion of concrete but plays a major role in determining the nature and influencing the behaviour and performance of concrete through the gradual hydration with cement particles. It greatly influences strength, stiffness and toughness.

To date, much attention has been paid to the study on strength and stiffness (RILEM 1985a, Phan & Carino 1998) at varied heating scenarios (heating rate, heating temperature, exposure time, cooling rate, etc.). Besides strength and stiffness, the fracture energy is a very useful fracture toughness parameter for designing and manufacturing high strength high performance concrete materials and analysing structural behaviour under varied loading and environmental conditions. Bazant & Prat (1988) conducted three-point bending and eccentric compression tests on both dry and saturated concrete specimens heated up to 200°C and found that the fracture energy monotonically decreased with increasing temperature and that saturated specimens yielded much smaller fracture energy. Based on the three-point bending tests on short concrete beams thermally shocked or slowly cooled, Baker (1996) found that the fracture energy first increased with increasing temperature until a transition point was reached and gradually decreased thereafter. The slowly cooled specimens showed higher values of the fracture energy. Felicetti et al. (1996) measured the fracture energy on the concrete specimens pre-heated up to 500°C under three-point bending and direct tension, but the test results showed no significant change in fracture energy. The authors (2000a) investigated the

effects of heating temperature, exposure period and curing age on the residual fracture energy of the normal- and high-strength concrete by conducting three-point bending tests on the notched pre-heated beams. The fracture energy increased with heating temperature until 300°C and decreased thereafter. Longer exposure time leads to an increase of fracture energy at lower temperatures and to a decrease at higher temperatures. Fracture energy also increased with the curing age. Authors also used different toughness indices to quantitatively assess the toughness of concrete at high temperatures and found the toughness increased with increasing heating temperature and exposure time, but slightly decreased with curing age (Zhang et al. 2000b, c). So far, little work has been done to measure the fracture energy of concrete at high temperatures (i.e. while the concrete is *hot*). Hence, more work needs to be done to further study the effect of varied heating scenarios on the fracture energy of concrete at high temperatures. Also the effect of moisture migration on the fracture energy needs to be further investigated.

In this study, the effects of the heating temperature T_m and the cooling manner on the fracture properties of concrete were investigated by conducting three-point bending tests on the notched beams of high performance concrete in a furnace. Beside fracture energy G_F as a primary parameter, compressive strength f_{cu}, splitting tensile strength f_t', modulus of rupture f_r and Young's modulus E were also studied. G_F and f_r were measured under both *hot* and *cold* conditions, whereas other properties were measured after cooling (residual). The weight loss ω was continuously measured during the time when the concrete was heated and could be used to further study its effect on the fracture behaviour of concrete during heating. Thus, the relationships of G_F and other properties with T_m, cooling ways and ω could be established.

2 EXPERIMENTAL

Eight heating temperatures were used (T_m = 105, 150, 200, 250, 300, 350, 400 and 450°C) with a constant heating rate of 3°C/min for a fixed exposure time of 16 hours. Cooling was obtained by leaving the furnace either closed (slow cooling) or fully open (fast cooling). For reference, five beams were tested at room temperature (20°C). At least three beams were tested for each heating scenario. Thus, a total of 101 beams were tested in this study.

Notched concrete beams of 500 × 100 × 100 mm, with an effective span of 400 mm and a notch depth of 50 mm, were loaded in three-point bending to determine G_F. The beams were notched before they were heated using a diamond saw. A beam length of 500 mm rather than 840 mm as recommended by RILEM (1985b) was chosen to suit the internal di-

mensions of the furnace. Brokenshire & Barr (1995) found no noticeable difference in measuring G_F due to such size change. Sixty prisms of 200 × 100 × 100 mm were also cast to determine the residual Young's modulus. Some heated beams were cut after bending tests into 100 mm cubes for residual strength tests.

The cement was ordinary Portland cement (OPC) of class 42.5N. Pulverised Fuel Ash (PFA) was used to reduce the porosity and make high performance concrete. The sand was the calcareous quartz sand and the coarse aggregates were the 10 mm single-sized (CA1) and 20 mm graded (CA2) quartz dolerite (basalt type). Pozzolith 300 N plasticiser was used to reduce water content and obtain a high slump of 125 mm. The concrete mixes are listed in Table 1. The test age was at least 90 days to allow full hydration, giving f_{cu} = 67.1 MPa. f_t' = 4.47 MPa and E = 35.64 GPa.
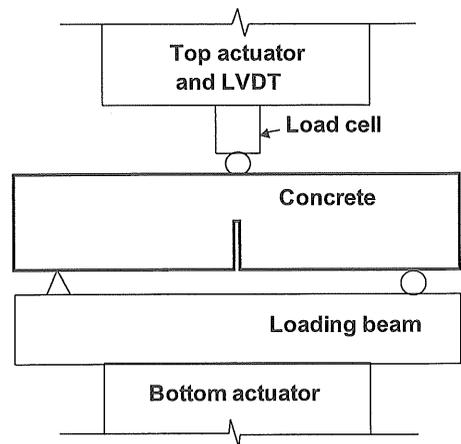

Figure 1. Test arrangement in this study.

Table 1. Concrete mixes.

Content	Ratio	Quantity
		kg/m³
Cement	1.00	300
PFA	0.33	99
Sand	2.45	735
10 mm aggregate	1.39	417
20 mm aggregate	2.78	834
Water	0.56	168
Plasticiser	0.006	1.8

A program-controlled VTS furnace (600 ± 5°C) was designed for this project, including two identical halves and three independent heating zones to help to heat the concrete uniformly. Fans were used to circulate the air in the furnace and as well as to cool the loading pieces connected to the actuators. The furnace was built around the 2000 kN LOS universal

testing machine so as to allow the tests to be conducted at high temperatures. A loading piece made of high-yield steel was specially manufactured to allow two beams to be tested while being *hot* from one heating batch. A 10 kN high temperature load cell (working temperatures up to 180°C) was used to measure the load at high temperatures. The displacement of the testing machine was automatically measured and used for calculating G_F. The three-point bending tests were conducted at a displacement rate of 1.25×10^{-3} mm/s.

For continuous monitoring of the moisture migration during heating, two steel cradles were produced for hanging concrete beams. Each cradle was connected to a 25 kg high precision load cell via a steel bar. During the complete heating process, the weight was continuously monitored and regularly recorded. A factory balance of 15 kg $\pm$ 5g was used to measure the concrete weight before heating and after cooling to obtain the ultimate weight loss. Thermocouples were fixed either on the surface or in the centre of the concrete beams to monitor the temperature evolution.

f_{cu} and f_t' were obtained on at least six 100 mm cubes and E on four 200 × 100 × 100 mm prisms for each heating scenario.

3 WEIGHT LOSS

3.1 *Weight loss ω through complete heating process*

Figure 2 shows the continuous developments of the weight loss through the complete heating, exposure and slow cooling process. ω is a monotonically increasing function of heating time t through three stages. In the first stage, ω increased very little with t at a small increase rate because heat could only evaporate the moisture near the concrete surface. The ω - t curves are concave, and this stage lasted a few hours. In the next stage, the moisture evaporated very quickly and consequently ω increased very rapidly with t. The rate of increase became gradually larger and then decreased after a maximum was reached, the corresponding ω - t curves becoming convex. The temperature also became gradually uniform in the concrete and drove out the moisture from further depth. This stage would last shorter with increasing T_m, 16 hours for 150°C but only 3 hours for 300°C and 450°C. At the third stage, the rate of evaporation became smaller again so ω slightly increased with t at a decreased rate, eventually reaching its ultimate value. The moisture level within the furnace chamber may have reached the hygric steady state as well.

3.2 *Weight loss for different heating temperatures*

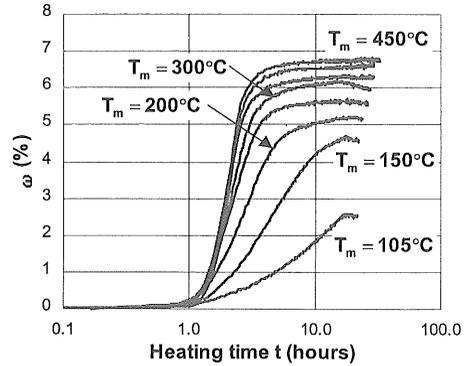Figure 2 also shows that at any heating stage, a higher heating temperature always led to a higher

Figure 2. Weight loss through the complete heating process.

weigh loss. If the exposure time is long enough, both thermal and hygric equilibrium states could be reached with an ultimate weight loss ω_u. At 105°C and 150°C, a slightly longer exposure time up to 16 hours may be needed to reach the equilibrium state. For higher temperatures, ω only increased in the first few hours and then tended to reach ω_u. Figure 3 shows that ω_u increased bi-linearly with T_m. At the start, ω_u increased significantly with T_m until 150°C. This stage can be regarded as a predominantly physical process, associated with the evaporation of capillary water in concrete as water escapes from these macro capillary pores. With the increase of T_m, ω_u kept increasing at a smaller rate and the further weight loss was mainly caused by the evaporation of gel water. The smaller evaporation rate was due to the difficulty for gel water to escape from gel pores. This stage can be described as a physical-chemical process. Normally there should be a third stage where the further weight loss would be mainly due to the dehydration and decomposition of hardened cement paste and aggregates, referring to a predominantly chemical process due to evaporation of micro chemically combined water. Because the heating temperature was only up to 450°C, the third stage was not reached or was not very obvious.

3.3 *Weight loss for different cooling rates*

Figure 3 also shows no difference in ω_u between slow and fast cooling because the thermal gradient within the concrete was not large. However, the fast cooling would cause a large thermal gradient and absorbs the moisture in the air into the concrete. Thus, a lightly smaller weight loss was expected for the fast cooling.

Normally larger negative thermal gradient absorbed more moisture from the air into the concrete during fast cooling, but it also disappeared quickly so the absorbing time became shorter. Consequently, less water would be absorbed for fast cooling. Slow
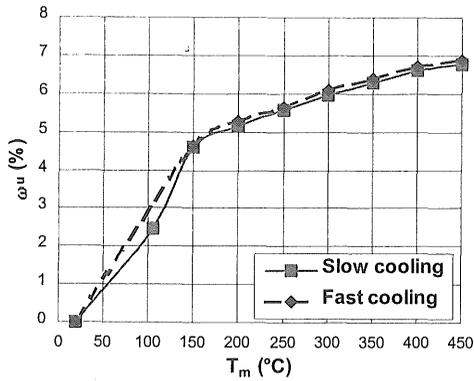
Figure 3. Ultimate weight loss for different heating temperatures.

cooling allowed a longer absorbing time so a slightly lower weight loss could be expected. Typically, ω_u was 4.6% for both slow and fast cooling at 150°C, 6.0% for slow cooling and 6.1% for fast cooling at 300°C, and 6.8% for slow cooling but 6.9% for fast cooling at 450°C. This means very little influence of the cooling rate on the ultimate weight loss.

4 FRACTURE ENERGY

Fracture energy G_F, defined as the total energy dissipated over a unit crack area, was obtained on the basis of the work done by the force (the area under a load-displacement curve in three-point bending on a centrally notched beam) associated with the gravitational work done by the self-weight of the beam.

4.1 Fracture energy for different heating temperatures

Figure 4 shows the fracture energy from the three-point bending tests on both *hot* and *cold* beams. The heating temperature at testing greatly influenced G_F. For the *hot* concrete, G_F sustained a decrease-increase process with T_m. G_F first decreased from 230 N/m at 20°C to 208 N/m at 105°C and reached its minimum of 193 N/m with a net drop of 37 N/m or 16%. This was mainly caused by the high vapour pressure inside the concrete, because the moisture could not efficiently evaporate at low heating temperatures and remained inside the concrete, forming the high hygric gradients. A higher humidity generally reduces the resistance of concrete against failure. With the further increase of T_m, G_F started to recover and continuously increased because the moisture could more freely escape. A higher T_m could make the concrete softer and more ductile. Hence, more energy would be consumed to break a concrete beam when it was hot. G_F increased to 214

N/m at 200°C and fully recovered to 238 N/m at 250°C. It kept increasing to 261 N/m at 300°C, 292 N/m at 400°C and eventually 305 N/m at 450° with a net increase of 75 N/m or 33%.
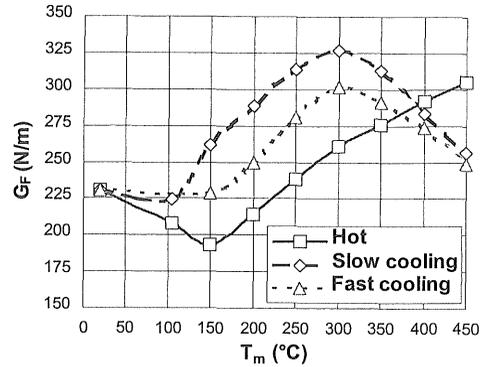

Figure 4. Fracture energy for different heating temperatures.

For the beams under slow and fast cooling, G_F had a hold-increase-decrease trend. G_F first slightly decreased at 105°C and then started to increase with T_m until 300°C. A heating temperature under 300°C appeared to help further hydration of cement paste and strengthen the interface so as to raise the resistance against cracking and failure. However, higher heating temperatures cause more micro-cracks, dehydration and decomposition so as to degrade material resistance. G_F continuously decreased with T_m after 300°C. The final figure for G_F was still larger than the reference value for G_F at room temperature.

4.2 Fracture energy for different cooling rates

Figure 4 also shows that the G_F - T_m curves for slow and fast cooling followed similar trends. Another consistent feature is that the G_F - T_m curve for fast cooling is always below that for slow cooling. This means that fast cooling caused more extensive damage to concrete so lower fracture energy could be expected.

Under slow cooling, G_F first slightly decreased to 225 N/m at 105°C. Then it started to increase with T_m to 261 N/m at 150°C and 289 N/m at 200°C and reached its ultimate of 327 N/m at 300°C with a net increase of 97 N/m or 42%. Under fast cooling, G_F was almost unchanged at 150°C and then started to increase with T_m to 249 N/m at 200°C and to its maximum of 327 N/m at 300°C with a net increase of 97 N/m or 42%. Thereafter G_F continuously decreased with T_m after 300°C and dropped down to 256 N/m under slow cooling and 249 N/m under fast cooling at 450°C. The final figures were still larger than the value at room temperature.

G_F was smaller for the *hot* concrete when $T_m \le$

350°C but became larger when when $T_m > 350°C$. Summary from these three sets of results indicates a smallest G_F on the *hot* concrete, followed by that on the fast cooled concrete and on the slow cooled concrete if T_m was under 400°C. For even higher heating temperatures, the order would change to: fast cooled, slow cooled and *hot* concrete.

4.3 *Fracture energy versus ultimate weight loss*

Figure 5 shows the relationship of G_F with ω_u for both *hot* and *cold* concrete. The reference fracture energy at room temperature is also included corresponding to the zero weight loss. For the *hot* concrete, G_F first slightly decreased with ω_u until a transition weight loss ω_{u1} was reached and then continuously increased. ω_{u1} was 4.6% and corresponded to 150°C. Because of very dense concrete with smaller capillary pores in this study, the moisture could not be easily removed from capillary pores at this stage until a higher heating temperature was applied. The removal of moisture from the concrete slightly reduced the fracture energy of the *hot* concrete. Thereafter the evaporation of capillary water and even gel water made the concrete tougher while tested at higher temperatures, due to the gradual disappearance of the lubricating effect of the water inside the concrete. A bi-linear $G_F - \omega_u$ relationship can be used for the *hot* concrete.
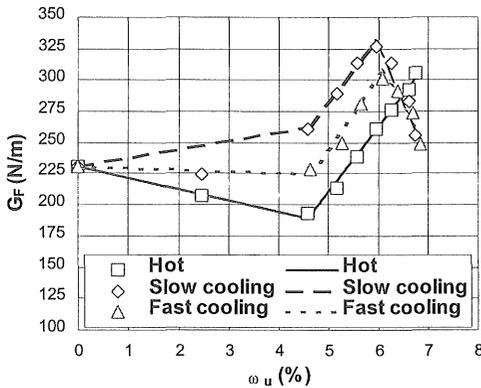

Figure 5. Fracture energy versus ultimate weight loss.

G_F sustained a hold-increase-decrease tendency with ω_u for the *cold* concrete In the first stage, G_F only slightly increased for slow cooling or changed little for fast cooling until ω_{u1} was reached at 150°C because the damage to the concrete caused by the vapour pressure during heating eliminated the toughening effect associated with the weight loss. In the second stage, G_F increased at a higher rate until another transition weight loss ω_{u2} was reached. ω_{u2} was 6.0% for slow cooling and 6.1% for fast cooling and

corresponded to 300°C. This stage was accompanied with further evaporation of the capillary water and is a physically dominant process. Gradual removal of the capillary water further reduces the lubricating effect of the water and toughens the concrete. G_F - ω_u curves were also almost parallel to one another for different cooling rates. In the final stage, G_F decreased continuously with ω_u, accompanied with the evaporation of gel water and chemically combined water and even decomposition and this process is dominated by chemical reactions. Cooling process significantly damaged the concrete and decreased the fracture energy even though the weigh loss was not affected too much. Here ω_{u1} and ω_{u2} depend not only on concrete composition but also on heating scenarios. The $G_F - \omega_u$ curves for slow and fast cooling could be multi-linear, as shown in Figure 5.

5 MODULUS OF RUPTURE

The modulus of rupture f_r was directly calculated from the ultimate load, measured on both *hot* and *cold* concrete beams. Figure 6 shows the values of f_r for varied heating temperatures. For the *hot* concrete, f_r sustained a decrease-recovery-decrease tendency but generally followed a decreasing trend with increasing T_m. f_r decreased from 6.2 MPa at 20°C to 4.8 MPa at 105°C due to the high vapour pressure inside the concrete, with a sudden drop of 23%, and then recovered to 6.2 MPa at 200°C. Thereafter it continuously decreased to 5.9 MPa at 300°C and 5.3 MPa at 450°C with a net drop of 15%.
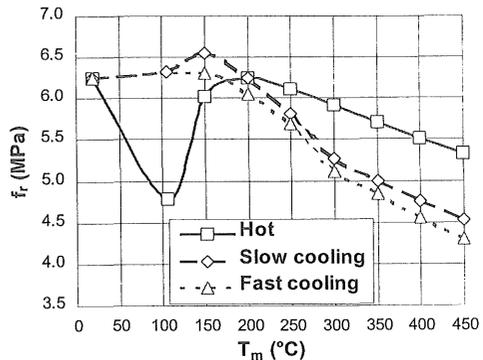

Figure 6. Modulus of rupture at different heating temperatures.

For the *cold* concrete, f_r slightly increased until the 150°C level and then continuously decreased with T_m. f_r slightly increased at 150°C and then continuously decreased. At 450°C, f_r was 4.5 MPa for slow cooling and 4.3 MPa. The corresponding drops of 27% and 31% were much larger than that on the *hot* concrete, which means that cooling process

465

caused further damage to the concrete by forming more micro-cracks.

The loading capacity under fast cooling was always lower than the one under slow cooling at all heating temperatures, but the difference between two ultimate loads at any T_m was smaller than 0.3 MPa.

Figure 7 shows the relationship of f_r with ω_u. For the *hot* concrete, f_r had a decrease-recovery-decrease trend with ω_u. f_r sharply decreased with ω_u first to 4.8 MPa at 105°C with a strength loss of or 24%, corresponding to $\omega_u = 2.5\%$. In the second stage, f_r quickly recovered back to 6.2 MPa at 200°C with $\omega_u = 5.2\%$. Thereafter, f_r decreased with ω_u again.
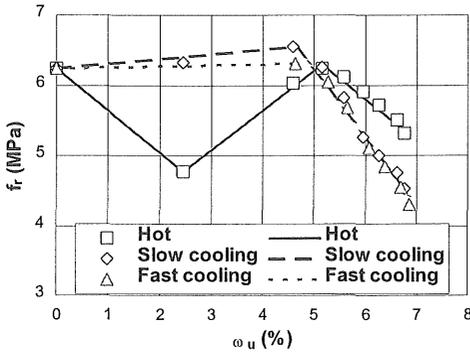

Figure 7. Modulus of rupture versus ultimate weight loss.

For the *cold* concrete, f_r sustained an increase-decrease tendency with ω_u. It slightly increased with ω_u until 150°C with $\omega_{ul} = 4.6\%$ and then continuously decreased with ω_u. The f_r - ω_u relationships for different stages on the *cold* concrete could be approximated as bi-linear, as shown in Figure 7.

6   RESIDUAL CONCRETE STRENGTHS

Figure 8 shows both f_{cu} and f_t' had similar decrease-recovery-decrease trends with T_m. They first sharply decreased at 105°C and then slightly recovered. Thereafter they continuously decreased. For slow cooling, f_{cu} decreased from 67.1 MPa at 20°C to 55.2 MPa at 105°C, with a sudden drop of 11.9 MPa or 18%, and recovered to 63.7 MPa at 200°C. Thereafter it continuously decreased to 60.9 MPa at 300°C and 53.8 MPa at 450°C with a net drop of 13.3 MPa or 20%. f_t' decreased from 4.5 MPa at 20°C to 3.4 MPa at 105°C, with a sudden drop of 1.2 MPa or 24%, but slightly recovered to 3.6 MPa at 150°C. Then it continuously decreased to 3.1 MPa at 300°C and 2.5 MPa at 450°C with a net drop of 2.0 MPa or 45%. f_t' had a loss 2.5 times larger than f_{cu}. This is because the tensile strength of concrete is mainly contributed to by the strength of cement paste and the interface bond strength with aggregates. The

compressive strength, however, is in addition also dependent on the interlock between the aggregates. It can also be seen that the f_t' - T_m curve was largely linear when T_m was above 150°C.
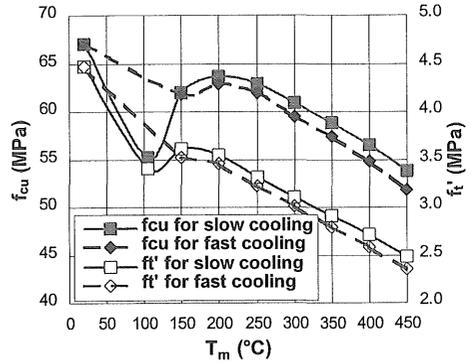

Figure 8. Concrete strengths at different heating temperatures.

Figure 8 also shows f_{cu} and f_t' had the same trends with T_m under fast cooling, but the corresponding f_{cu} - T_m and f_t' – T_m curves were always lower. This means that fast cooling led to even smaller concrete strengths. When T_m was below 200°C, the differences in f_{cu} and f_t' were small but became gradually larger with the increase of T_m, which means that fast cooling at higher temperatures led to even smaller strengths due to the larger thermal gradients.

Figure 9 shows decrease-recovery-decrease trends of f_{cu} and f_t' with ω_u. For slow cooling, f_{cu} first sharply decreased with ω_u to 55.2 MPa at 105°C with $\omega_u = 2.5\%$ but gradually recovered to 63.7 MPa at 200°C with $\omega_u = 5.2\%$. Thereafter it continuously decreased with ω_u. f_t' also sharply decreased with ω_u from 4.5 MPa to 3.4 MPa at 105°C but recovered to 3.6 MPa at 150°C with $\omega_u = 4.6\%$ and unchanged up to 200°C. Then it continuously decreased with ω_u. Figure 9 also shows that both f_{cu} - ω_u and f_t' - ω_u curves for slow and fast cooling followed the same trend. The only difference is that the strengths - ω_u curves for fast cooling are slightly lower. However, this difference became too small to be distinguished when ω_u was higher than 5%. Both f_{cu} and f_t' under fast cooling should have the same three-stage trends with ω_u. Because no test data were available for $T_m = 105°C$, the first two stages became unclear. By the end of the second stage, f_{cu} recovered to its peak of 62.9 MPa at 200°C with $\omega_u = 5.3\%$. f_t' reached its peak of 3.5 MPa at 150°C with $\omega_u = 4.6\%$. In the third stage, both f_{cu} and f_t' rapidly decreased with ω_u.
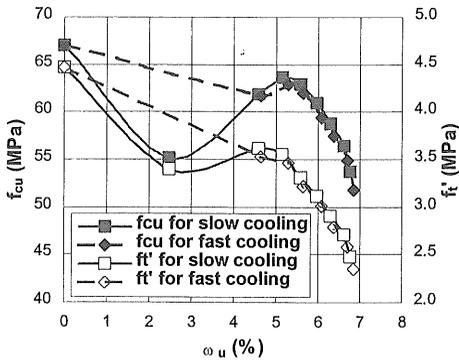
Figure 9. Concrete strengths versus ultimate weight loss.

7 RESIDUAL YOUNG'S MODULUS

Figure 10 shows that the residual Young's modulus of the concrete under slow and fast cooling decreased almost linearly with the increasing heating temperature. This is because a higher heating temperature always caused a higher migration of moisture from the concrete and also reduced the stiffness of cement paste and aggregates. E continuously decreased from 35.6 GPa at room temperature to 27.0 GPa at 150°C, 17.6 GPa at 300°C and finally 10.0 GPa at 450°C with a significant loss of 25.6 GPa or 72%. There was no obvious difference in E between the slow and the fast cooling. Fast cooling seemed to lead to a slightly lower E, but this difference was too small to be distinguished. The E - T_m curves for slow and fast cooling could be expressed using a single linear relationship. This means that the manner of cooling in this study did not influence the E - T_m relationship.

Figure 11 shows the residual Young's modulus versus ultimate weight loss relationships for the concrete under slow and fast cooling. E sustained a two-stage monotonic decrease tendency with ω_u. In the first stage, E decreased slowly with ω_u until a transition point was reached and then went down much more rapidly. The decrease rate in the second stage was four times as large as that in the first stage. These two stages corresponded to the cases at lower and higher heating temperature, respectively. In the first stage relatively low heating temperatures could only evaporate the capillary water from the concrete and did not greatly influence the stiffness of the cement paste and aggregates. In the second stage, however, relatively higher heating temperatures not only evaporated the gel water and the chemically combined water and caused decomposition, but also reduced the stiffness of the cement past and aggregates. Thus, a smaller increment in ω_u in this stage would always be accompanied with the degradation of cement paste and aggregates and their interface.

Figure 11 also shows the E - ω_u curves for slow and fast cooling coincided with each other and could be simply expressed using a single bi-linear equation.
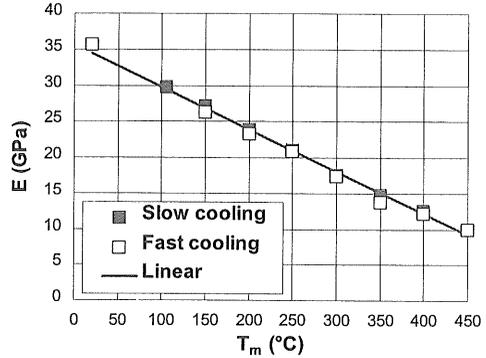

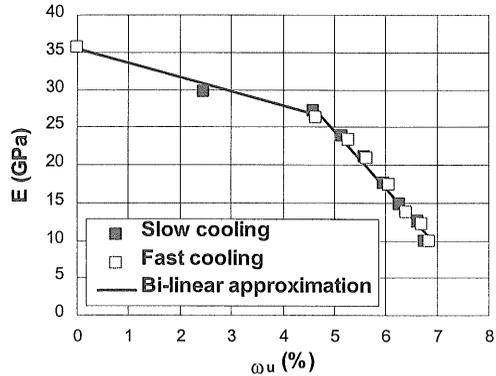Figure 10. Young's modulus for different heating temperatures.

Figure 11. Residual Young's modulus versus ultimate weight loss.

8 CONCLUSIONS

In this study, the effects of the heating temperature and cooling rate on the fracture energy and other materials properties of the *hot* and *cold* concrete. The following conclusions can be drawn:

Weight loss monotonically increased with the heating temperature but a hygric equilibrium state could be reached if the exposure time was kept long enough. Fast cooling led to a slightly higher ultimate weight loss.

Fracture energy generally sustained a decrease-increase tendency with the heating temperature for the *hot* concrete but an increase-decrease tendency for the *cold* concrete. Fast cooling led to the lower fracture energy due to a large thermal gradient. Fracture energy changed with the ultimate weight loss in

a similar way to that with the heating temperature. A bi-linear decrease-increase relationship between fracture energy and the ultimate weight loss for the *hot* concrete could be found but a tri-linear hold-increase-decrease relationship showed a good approximation for the *cold* concrete. In the first stage, the evaporation of capillary water at lower heating temperatures only slightly affected the fracture energy of concrete but the later evaporation of gel water and chemically combined water and even decomposition significantly reduced the fracture energy.

Modulus of rupture representing the loading capacity of concrete under bending generally decreased with the increasing heating temperature for the *hot* concrete, but sustained an increase-decrease tendency for the *cold* concrete. There was a sudden drop at 105°C for the *hot* concrete due to high vapour pressure inside the concrete. Fast cooling only slightly decreased the modulus of rupture. There existed a tri-linear decrease-recovery-decrease relationship between modulus of rupture and ultimate weight loss on the *hot* concrete and a bi-linear increase-decrease relationship on the *cold* concrete.

Both residual compressive and tensile strengths decreased with the increasing heating temperature and cooling rate. There was a sudden drop in the concrete strengths between 105°C and 150°C due to the residual stress caused by the high vapour pressure inside the concrete. Tensile strength decreased more rapidly than compressive strength for the same heating scenario. Concrete strengths had two-stage decrease trends related to the ultimate weight loss.

Residual Young's modulus of concrete monotonically decreased with increasing heating temperature but was hardly influenced by the cooling rate. There existed a two-stage linear relationship between Young's modulus and the ultimate weight loss.

ACKNOWLEDGEMENTS

REFERENCES

Baker, G. 1996. The effect of exposure to elevated temperatures on the fracture energy of plain concrete. *RILEM Materials and Structures* 29: 383-388.

Bazant, Z.P. & Kaplan, M.F. 1996. *Concrete at High Temperatures: Material Properties and Mathematical Models*. Harlow Essex: Longman Group Limited.

Bazant, Z.P. & Prat, P.C. 1988. Effect of temperature and humidity on fracture energy of concrete. *ACI Materials Journal* 85(4): 262-271. July-August.

Brokenshire, D.R. & Barr, B.I.G. 1995. A comparative study of G_F test results. In Wittmann F.H. (ed.), *Proc. of the 2nd Inter. Conf. on Fract. Mech. of Concr. Struct. (FRAMCOS 2)*: 3-16. ETH Zurich, Switzerland, July 25-28.

Felicetti, R., Gambarova, P.G., Rosati, G.P., Corsi, F. & Giannuzzi G. 1996. Residual mechanical properties of high-strength concretes subject to high-temperature cycles. *4th Inter. Synopsis on Utilisation of High Strength/High Performance Concrete*: 579-588. Paris.

Phan, L.T. & Carino, N.J. 1998. Review of mechanical properties of HSC and elevated temperature. *Journal of Materials in Civil Engineering, ASCE* 10(1): 58-64. February.

RILEM Committee 44-PHT. 1985a. Behaviour of concrete at high temperatures. Schneider U. (ed.), Dept. of Civil Engineering, Gesamthochschule, Kassel University, Kassel (Germany): 122 pp.

RILEM Technical Committe 50 FMC. 1985b. Draft recommendation: determination of the fracture energy of mortar and concrete by means of three-point bend test on notched beams. *RILEM Materials and Structures* 18(107): 407-413.

Schneider, U. 1988. Concrete at high temperatures - a general review. *Journal of Fire Safety* 13: 55-68.

Zhang, B., Bicanic, N., Pearce. C.J. & Balabanic G. 2000a. Residual fracture properties of normal and high-strength concrete subject to elevated temperatures. *Magazine of Concrete Research* 52(2): 123-136.

Zhang, B., Bicanic, N., Pearce. C.J. & Balabanic G. 2000b. Assessment of toughness of concrete subject to elevated temperatures from complete load-displacement curve – part I: general introduction. *ACI Materials Journal* 97(5): 550-555. September-October.

Zhang, B., Bicanic, N., Pearce. C.J. & Balabanic G. 2000c. Assessment of toughness of concrete subject to elevated temperatures from complete load-displacement curve – part II: experimental investigations. *ACI Materials Journal* 97(5): 556-566. September-October.